PNAS RESEARCH ARTICLE | MICROBIOLOGY OPEN ACCESS

Breaking down antibiotic resistance in methicillin-resistant *Staphylococcus aureus*: Combining antimicrobial photodynamic and antibiotic treatments

Jace A. Willis[a], Vsevolod Cheburkanov[a], Shaorong Chen[b], Jennifer M. Soares[c], Giulia Kassab[c], Kate C. Blanco[a,c], Vanderlei S. Bagnato[a,c,1], Paul de Figueiredo[b,d], and Vladislav V. Yakovlev[a]

Contributed by Vanderlei S. Bagnato; received May 15, 2022; accepted July 27, 2022; reviewed by Edward De Robertis and Merrill Biel

The widespread use of antibiotics drives the evolution of antimicrobial-resistant bacteria (ARB), threatening patients and healthcare professionals. Therefore, the development of novel strategies to combat resistance is recognized as a global healthcare priority. The two methods to combat ARB are development of new antibiotics or reduction in existing resistances. Development of novel antibiotics is a laborious and slow-progressing task that is no longer a safe reserve against looming risks. In this research, we suggest a method for reducing resistance to extend the efficacious lifetime of current antibiotics. Antimicrobial photodynamic therapy (aPDT) is used to generate reactive oxygen species (ROS) via the photoactivation of a photosensitizer. ROS then nonspecifically damage cellular components, leading to general impairment and cell death. Here, we test the hypothesis that concurrent treatment of bacteria with antibiotics and aPDT achieves an additive effect in the elimination of ARB. Performing aPDT with the photosensitizer methylene blue in combination with antibiotics chloramphenicol and tetracycline results in significant reductions in resistance for two methicillin-resistant *Staphylococcus aureus* (MRSA) strains, USA300 and RN4220. Additional resistant *S. aureus* strain and antibiotic combinations reveal similar results. Taken together, these results suggest that concurrent aPDT consistently decreases *S. aureus* resistance by improving susceptibility to antibiotic treatment. In turn, this development exhibits an alternative to overcome some of the growing MRSA challenge.

photodynamic therapy | antibiotic resistance | antimicrobial-resistant bacteria | methicillin-resistant *Staphylococcus aureus* | methylene blue

Significance

Antimicrobial-resistant bacteria (ARB) are a present and growing healthcare threat, especially for hospitalized patients where nosocomial infections constitute a growing concern. Methicillin-resistant *Staphylococcus aureus* (MRSA), for example, has posed a significant risk for hospital-associated illness since its discovery (M. P. Jevons, 1961). The tools most used to fight resistant pathogens involve multiple antibiotics, synthetic antibiotic hybrids, or a combination with an adjuvant to increase susceptibility. Utilization of antimicrobial photodynamic therapy (aPDT) provides nonspecific impairment of resistance mechanisms, diversifying the appropriate antibiotics and reducing necessary doses. Here, combined aPDT and antibiotic treatment is demonstrated in vitro against multiple MRSA strains, yielding increased antibiotic susceptibility. This presents an opportunity to extend the efficacious lifetime of existing antibiotics.

Antimicrobial-resistant bacteria (ARB) have raised public health concerns since the beginning of industrial antibiotic production in the 1940s (1). Healthcare-associated infections with ARB have caused significant morbidity, mortality, and economic burdens (2). In fact, according to the Centers for Disease Control and Prevention, over 2.8 million ARB infections occur every year, resulting in more than 35,000 deaths in total (3). Although many bacterial pathogens are successfully treated with antibiotic therapies, the treatment itself is the leading source of increasing antimicrobial resistance (4). The treatment methods for ARB most commonly involve the use of combination antibiotic therapies or treatment with adjuvants that target bacterial resistance mechanisms, including efflux pumps (5). These treatments are primarily beneficial due to their specific effectiveness against antimicrobial-resistant organisms but include moderate to severe undesired side effects such as neurotoxicity, kidney damage, and myelosuppression (6–8). Those who acquire ARB infections are much more likely to develop severe symptoms leading to poorer outcomes than those who acquire non-ARB infections (9). Some levels of prevalence and transmission dynamics are understood and being explored by improved monitoring, such as the World Health Organization global antimicrobial resistance and use surveillance system, which aid proper type and deployment of preventative measures. Nonetheless, a long-term solution to infection with diverse ARB has yet to be identified and serves as the ultimate goal.

Antimicrobial photodynamic therapy (aPDT) is a technique by which pathogens are inactivated by reactive oxygen species (ROS) generated from the coincidence of molecular oxygen, a photosensitizer, and characteristic light of a particular wavelength (10). The resulting ROS may cause nonspecific biological oxidative stress (11). Additionally, noncytotoxic photosensitizers have been shown to influence specific drug localization and photoactivation wavelengths, corresponding to control of aPDT activation depth in tissues (12). The absorption spectrum of methylene blue, with a maximum molar absorptivity of 85,000 M^{-1} cm^{-1} at 664 nm, is concentration-dependent to dimerization and proportional to ionic strength at interfaces. The quantum yield of methylene

Author contributions: J.A.W., V.C., S.C., J.M.S., G.K., K.C.B., V.S.B., P.d.F., and V.V.Y. designed research; J.A.W. and V.C. performed research; S.C. provided technique guidance; J.A.W. and V.C. analyzed data; and J.A.W. wrote the paper.

Reviewers: E.D.R., University of California, Los Angeles David Geffen School of Medicine; and M.B., University of Minnesota Academic Health Center.

The authors declare no competing interest.

[1]To whom correspondence may be addressed. Email: vander@ifsc.usp.br.

Published August 29, 2022.

blue fluorescence is dependent on the solvent used, and its interactions display a low quantum yield (0.04) in water. However, the fluorescence signal of methylene blue is concentration- and aggregation-dependent, and reductions are observed when the molecule interacts with membranes, proteins, and other biological substrates that favor electron transfer reactions. Methylene blue can act in both type I and type II mechanisms depending on its aggregation state. Methylene blue undergoes reduction reactions after electronic excitation, generating semireduced radicals and promoting mitochondrial NAD(P)H oxidation. Leucomethylene blue generates high proton potentials, resulting in the generation of half of the $^1O_2$ radical species. The type II mechanism is favored in biological systems with higher oxygen concentrations in membranes than in water. The highest affinity of the molecule is for negatively charged interfaces, and melanin has been described in studies that illustrate methylene blue applications in dermatology. However, its quantum efficiency is reduced in tumors when administered intravenously (13).

aPDT treatments have demonstrated efficacy against numerous microorganisms in experimental animal models. Although many photosensitizers are FDA approved for other photodynamic applications such as cancer therapy, they have not been approved for aPDT applications against ARBs (14). Methylene blue biocompatibility is exploited for the treatment of methemoglobinemia. Membranes of diseased tissues have redox properties that facilitate methylene blue reduction or oxidation. Methylene blue can also easily permeate membranes through lipid bilayers (15).

Nevertheless, the promise of the approach has been demonstrated. For example, reports have shown that moderate aPDT doses eliminated most methicillin-resistant *Staphylococcus aureus* (MRSA) (16). Despite these advances, whether aPDT can offer potential benefits by reducing the doses required to combat ARB infection remains unresolved. If this were the case, the benefits associated with reduced antibiotic-associated side effects would be substantial. The radiation wavelength is normally chosen as the absorption peak of the molecule; this is the wavelength region of the most significant conversion of light energy into electronic energy of the molecule. Being electronically excited, the molecules are able, by collisional energy transfer, to produce the maximum number of ROS, thus maximizing the reactive effect of the photodynamic action. During clinical applications of aPDT, photosensitizers are usually administered systemically or topically. They are then activated by penetrating light greater than 600 nm in the therapeutic window of 600 to 800 nm (17). Wavelengths shorter than 600 nm are absorbed by hemoglobin, and wavelengths longer than 950 nm are absorbed by biological molecules that exhibit water vibration.

In this study, we tested the hypothesis that aPDT improves antibiotic treatment effectiveness against MRSA. We found that aPDT did indeed improve the efficacy of antibiotic treatment against clinical isolates of MRSA. Taken together, these data set the stage for further development of aPDT as a strategy for combatting ARB infections.

Results

The high-level concept of this study is presented graphically in Fig. 1. Typically, single antibiotic or aPDT treatments can be effective antimicrobial treatments, but this is not always the case. When antibiotics do not completely clear infections, the risk of emergence of antibiotic-resistant populations is increased. Although these resistant clones might be susceptible to higher antibiotic doses, such increases in dosing can lead to undesirable side effects. Similarly, aPDT can potentially select for photodynamically resistant microbes. Increased dosing of aPDT can also result in undesirable side effects. To remedy these shortcomings a combination treatment is proposed. This combination causes a reduction in antibiotic resistance allowing for smaller doses of both treatments to be used. As a result, microbes are more thoroughly eliminated, and the lower doses avoid undue side effects. The mechanism behind these effects is suspected to be due in part to the attraction of cationic methylene blue to the anionic membrane and associated efflux pumps, localizing the aPDT effect. This localized damage acts to both enable greater antibiotic entrance and impair antibiotic efflux activity, thereby lowering the necessary antibiotic dosage for microbial killing.

aPDT Significantly Reduces Tetracycline and Chloramphenicol MIC in *S. aureus*. Treatments of aPDT and antibiotics, Tet and Chl, were applied to *S. aureus* strains USA300 and RN4220 independently and in combination. These test groups included photosensitizer exposure, light exposure, aPDT, light with antibiotic, and aPDT with antibiotic (*Materials and Methods*). Evaluation of aPDT effects on antibiotic minimum inhibitory concentration (MIC) reveals significant reductions. Fig. 2 displays this effect on MIC in terms of $\log_2$(MIC) vs. total exposure. Each data point represents an independent MIC array result dependent on the total exposure. Dark controls with large concentrations of 10 mM methylene blue showed no significant variation from baseline growth. Methylene blue was selected for use in these experiments as a photosensitizing drug due to its reasonable biocompatibility (18) and absorption spectra centered on 650 nm (19).

Light controls in both strains did not vary significantly. However, aPDT-treated groups varied significantly from controls at exposures of 7.2 and 10.8 J/cm^2. For USA300, mean Chl MIC decreased from 32.0 to 5.03 μg/mL (i.e., > 6.36-fold) (Fig. 2). Similarly, mean Tet MIC decreased from 2.08 to 0.283 μg/mL (i.e., > 7.34-fold). Based on European Committee on Antimicrobial Susceptibility Testing (EUCAST 2021) Clinical Breakpoint Tables (20), *S. aureus* is considered resistant to Chl at concentrations above 8 μg/mL and susceptible at or below that point and is resistant to Tet at concentrations above 2 μg/mL and susceptible at or below 1 μg/mL. As such, the maximum aPDT treatment on *S. aureus* USA300 altered both Chl and Tet tolerance designations from resistant to susceptible. For RN4220, mean Chl MIC decreased from 29.3 to 6.70 μg/mL (i.e., > 4.37-fold), and mean Tet MIC decreased from 1.50 to 0.377 μg/mL (i.e., > 3.97-fold). At the maximum aPDT treatment, Chl tolerance remained in a susceptible designation but was reduced significantly, whereas Tet tolerance changed from an intermediate susceptibility designation to a fully susceptible designation. The above descriptions as fold changes in antibiotic susceptibility were further evaluated in comparison to gauge aPDT affects between strain–antibiotic combinations (Fig. 3).

aPDT was also applied in isolation to determine immediate elimination effects on bacterial populations (Fig. 4). This displays the reduction in bacterial colony-forming units per milliliter (CFU/mL) immediately after aPDT treatments. The effects of aPDT alone on bacterial populations are considered significant when inhibition is greater than 3 $\log_{10}$ CFU/mL. Only USA300 given 10.8 J/cm^2 surpassed limits for consideration as significant inhibition, reaching a loss of 3.49 $\log_{10}$ CFU/mL. RN4220 reached a maximum reduction of only 2.01 $\log_{10}$ CFU/mL, staying within bounds for significant inhibition. Although USA300 reaches outside of the limits and is not strictly considered nonlethal aPDT, since the follow-up test involves a long incubation,

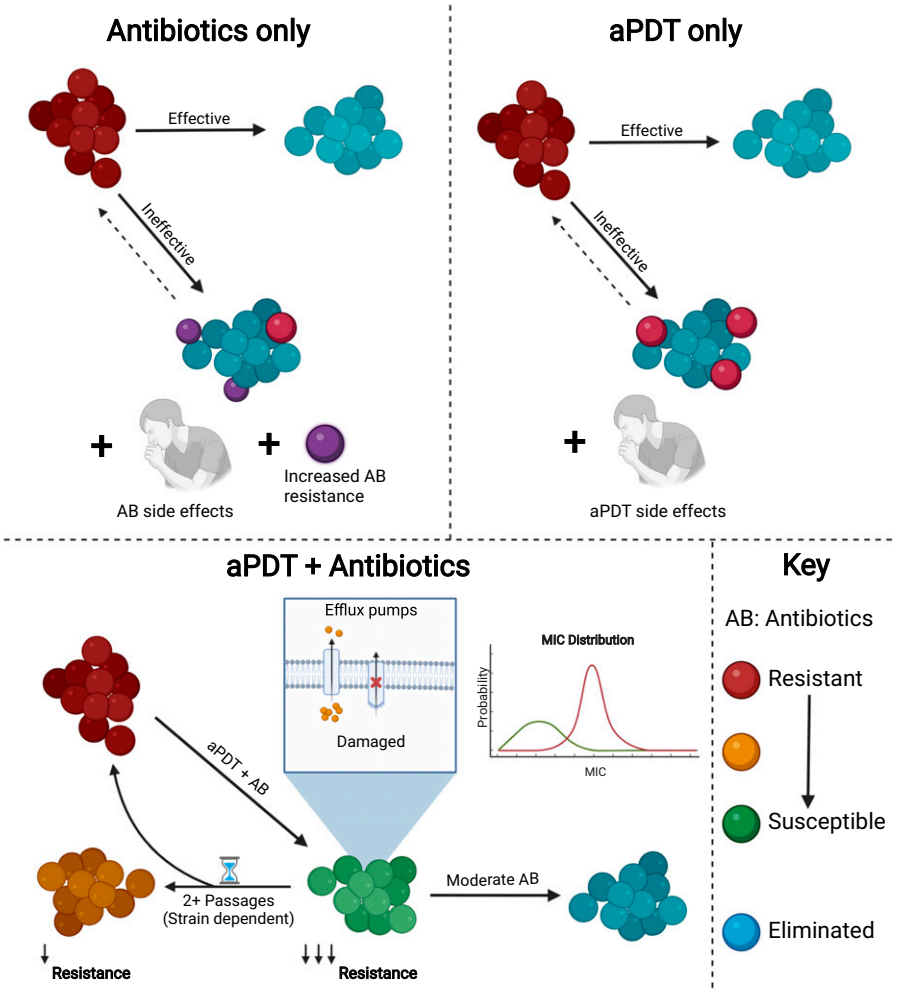

Fig. 1. Schematic representation of single and combined antibiotic and aPDT treatment options for infections. Antibiotics serve an important role in medicine, successfully treating many common bacterial infections. However, their use leads to increased resistance, necessitating more dangerous antibiotic classes and higher doses. Likewise, aPDT can successfully eliminate bacteria, regardless of antibiotic resistance, but is not always applicable at large doses due to drug and light side effects. These two treatments used concurrently have been found to significantly lower average antibiotic resistance and broaden the resistance distribution, permitting the use of smaller doses of each for a more effective treatment.

there is sufficient time to recover the population and not drastically affect antibiotic MIC results.

Determining the antibiotic susceptibility of various strains in the context of aPDT treatment was pursued to understand whether combination treatments can defeat antibiotic resistance.

Resistance Recovery over Serial Passages. It is clear that the addition of aPDT amplifies antibiotic effects on bacteria, but the residual effects on populations are vital to the understanding of the underlying mechanism and future treatment utility. As such, the same aPDT treatment groups were placed in 12-h cycling MIC culture plates where the most resistant of each triplicate was kept moving forward. In this way, the aPDT effects on MIC persistence could be determined in terms of serial passages. The initial aPDT MIC growth was considered to be passage 1.

Tet and Chl resistance of USA300 required two serial passages (12-h MIC; *Materials and Methods*) to return to baseline MIC values but was not entirely stable until passages 4 and 5. RN4220 also showed similarity between Tet and Chl resistance but did not return to baseline MIC values. In passage 3, RN4220 Tet and Chl MIC were stable at one-half of baseline and remained stable through passage 5. Therefore, it was concluded that residual effects on populations did not accumulate.

Additional Strains and Antibiotics Survey. Prior to in-depth testing of the above *S. aureus* strains, a series of wider selections of resistant *S. aureus* strains and antibiotics were surveyed. This survey examined aPDT interactions with the antibiotics ampicillin (Amp), kanamycin (Kan), tetracycline (Tet), and chloramphenicol (Chl). Strains examined included USA300, RN4220, ΔSaeR, MW2, and JE2. These survey results are summarized in Fig. 5.

The data gathered from Fig. 5 suggest that Tet and Chl are most likely to show results of interest in the average *S. aureus* strain. Meanwhile, Kan may or may not be of interest, and Amp rarely results in a synergistic response. Overall, these data are not meant to be interpreted as direct results, only to display how the selected combinations in Figs. 2–4 were decided and offer some perspective on one approach to this problem. Thus, data from experiments where aPDT was combined with antibiotic treatment of *S. aureus* strains led to the selection of the antibiotics Tet and Chl for further analysis of additive effects of combined treatments.

aPDT Acts Synergistically with Select Antibiotics and Strains. In combining the two treatments, the basic improvement of effectiveness is not sufficient to be classified as a synergy of effects. Rather, a standard metric such as the fractional inhibitory concentration index (FICI) is used to accurately gauge the

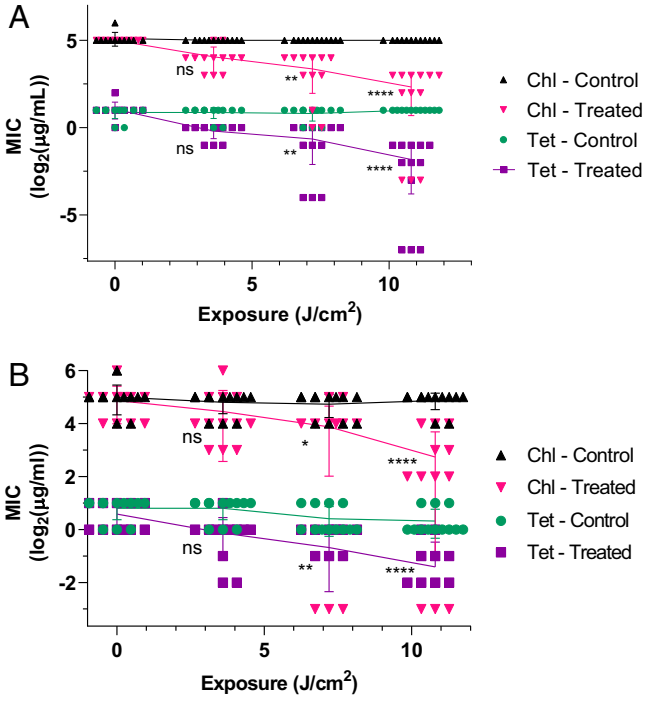

Fig. 2. Reduction in tetracycline (Tet) and chloramphenicol (Chl) MIC for *S. aureus* strains (*A*) USA300 and (*B*) RN4220 exposed to 0 to 10.8 J/cm^2 photoactivating light at 650 nm and containing 1 μM MB and 0.5 μM MB in the treated groups, respectively. "Control" denotes samples exposed to light but without PS, while "Treated" indicates the presence of PS in addition to light. For each sample series, distributions were compared with the Friedman's test and post hoc Dunn's multiple comparisons test relative to the no-exposure point. ns is not significant; *P < 0.05; **P < 0.01; ****P < 0.0001. Individual comparison P values are provided in Table 2. n = 12 for all samples.

effective value of combined treatments (21, 22). The FICI of any two treatments in combination is described by the addition of their fractional MICs or doses in combination divided by the same value when applied individually (Eq. **1**). The FICI matrix and key values are presented in Table 1 for the strains USA300 and RN4220, evidencing that for most of the combinations the result was additive in nature, with no group with an antagonistic result. The P-values for data corresponding to FICI calculations is given in Table 2.

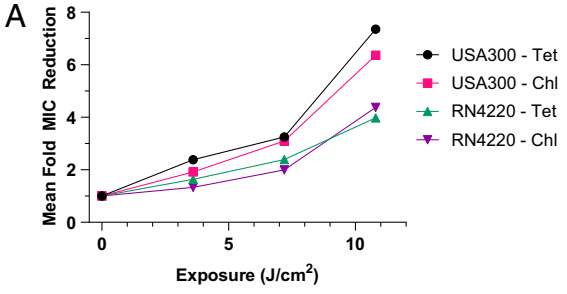

B

Exposure	USA300 – Tet	USA300 – Chl	RN4220 – Tet	RN4220 – Chl
3.6 J/cm^2	2.38	1.92	1.64	1.33
7.2 J/cm^2	3.25	3.10	2.39	2.00
10.8 J/cm^2	7.34	6.36	3.97	4.37

Fig. 3. (*A*) Mean antibiotic MIC concentrations from Fig. 2 where each exposure data point is divided by that sample's baseline MIC prior to exposure. (*B*) The same data are also given numerically for all mean fold MIC reductions as described in the above paragraphs. As only means are used in calculating fold MIC reduction, no statistical considerations can be made. n = 12 for all samples.

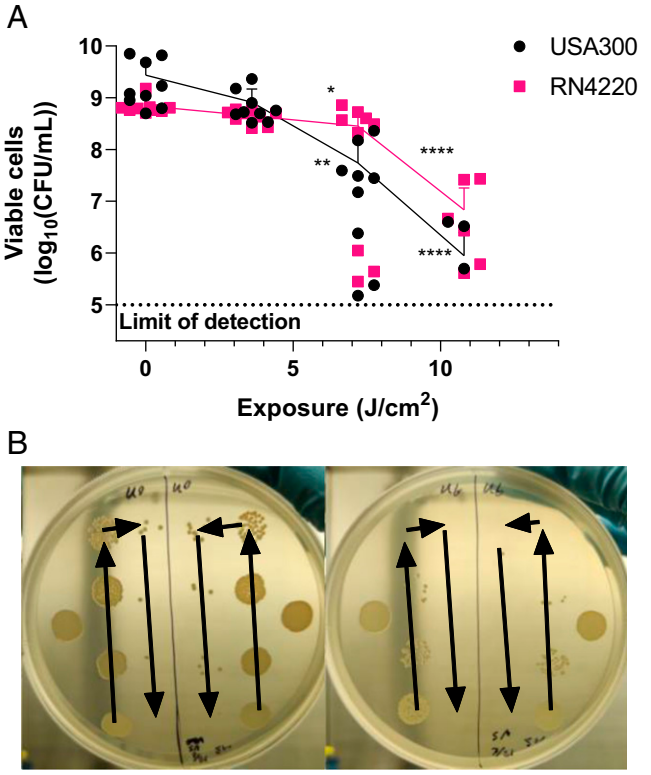

Fig. 4. Cultured assessment of viable cells [$\log_{10}$(CFU/mL)] immediately after aPDT treatment. (*A*) USA300 incubated with 1.0 μM MB and RN4220 incubated with 0.5 μM MB were exposed to 0 to 14.4 J/cm^2 photoactivating light. At 14.4 J/cm^2 exposure, both cultures were found to produce under the 10^5 CFU/mL limit of detec0074ion; thus, these data are not shown graphically. (*B*) An example of culture dishes is given, where arrows indicate the progressive twofold dilution of bacteria concentration by volume between spots. The left plate is USA300 given no light exposure, while the right plate is given 10.8 J/cm^2, both containing methylene blue. For each sample series of viable cells, distributions were compared with the Kruskal–Wallis test and post hoc Dunn's multiple comparisons test relative to the respective no-exposure point. ns is not significant; *P < 0.05; **P < 0.01; ****P < 0.0001. Individual comparison P values are provided in Table 2. n = 9 for all data points.

Therefore, we find here FICI values that describe the synergistic nature of aPDT and antibiotic combinations.

Discussion

Synergistic Treatment Effect and Mechanisms. The analysis of antibiotic susceptibility of ARB bacteria supports the hypothesis that moderate-dose aPDT significantly reduces resistance. ROS generated from aPDT cause indiscriminate damage, but the localization of photosensitizer by chemical characteristics acts as a focus (23). Cationic dyes such as methylene blue are localized more strongly to anionic structures such as membrane polymers (24), impacting transmembrane proteins that alter the flux of antimicrobial agents. Tet and Chl operate by inhibiting protein synthesis at ribosomal sites and therefore must cross the bacterial membrane to be effective. Bacteria photoinactivation using phenothiazinium has been demonstrated to display activity against vancomycin-resistant *Enterococcus* ssp, MRSA, and resistant bacterial biofilm structures. Several photosensitizer classes have been studied for their antimicrobial properties, such as Phenothiazinium (cationic and anionic) including methylene blue, toluidine blue, and rose bengal. Natural photosensitizers (neutral and cationic) such as curcumin, hypericin, flavin derivatives, and tetrapyrrole structures (cationic and neutral) act by applying porphyrin, phthalocyanine, and chlorine groups.

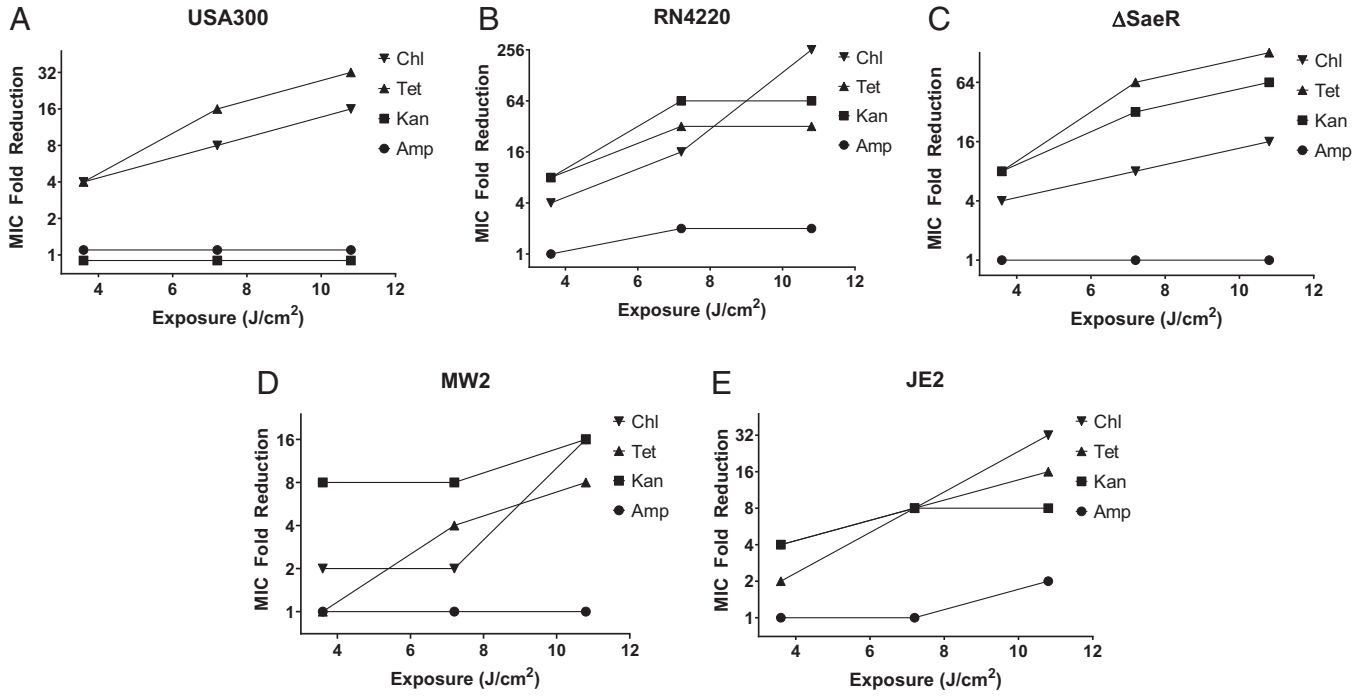

Fig. 5. aPDT treatment was combined with the antibiotics Amp, Kan, Tet, and Chl for the *S. aureus* strains (*A*) USA300, (*B*) RN4220, (*C*) ΔSaeR, (*D*) MW2, and (*E*) JE2. Each of the strain–antibiotic combinations was examined only once ($n = 1$) in this early survey trial. This surface-level observation was taken only to determine combinations of interest prior to more in-depth study. Each strain was tested with an MB concentration of 2 μM and was exposed to 0 to 14.4 J/cm^2 photoactivating light, but aPDT control cultures were completely eliminated at 14.4 J/cm^2, and thus, data stop at 10.8 J/cm^2. Since all data are single points, no statistical tests were completed.

Microbial toxicity rates have been found to typically be around 6 logs dependent on photosensitizer concentration, incubation time, and bacterial strain (gram-positive or gram-negative) (25). Bacterial resistance to these antibiotics may be related to impermeability, prevention, or transmembrane protein pumps, for removal (26). It is expected that the reduction in resistance achieved in this combined strategy occurs by an impairment of the bacterial membrane and corresponding resistance mechanisms, improving antibiotic uptake and diminishing efflux. Even if certain conditions are not sufficient to promote a change in the antibiotic susceptibility phenotype, our results demonstrate that aPDT increases the effectiveness of the antibiotic since lower doses of drugs are required to promote bacterial inactivation, so that certain classes of antibiotics can be extended in the pharmaceutical market using this strategy.

The recovery of antibiotic resistance over serial passages agrees with the above statements. USA300 recovered to complete baseline resistance as expected following membrane damage by aPDT and a constant presence of antibiotics. The delayed and incomplete recovery of RN4220 is reasonable due to nonspecific aPDT damage. In this scenario, the breakdown of resistance due to aPDT is not at the level of the genetic material; that is, it is not transmitted hereditarily but is sufficient to weaken cells temporarily. It is proposed that membrane damage is the primary mechanism of increased susceptibility short-term; however, aPDT also acts throughout the intracellular and extracellular space creating ROS and damaging biomolecules indiscriminately. As a result, the likelihood of other significant effects is nonnegligible, although they have not been thoroughly explored with respect to antibiotic resistance. This may suggest that there may be nonmembrane damage to resistance mechanisms that are not completely recovered over multiple generations.

Table 1. Calculated FICI values for *S.* aureus strains USA300 and RN4220 given ranges of aPDT and antibiotic treatments Tet and Chl

Light dose (J/cm^2)	USA300: Tet	USA300: Chl	RN4220: Tet	RN4220: Chl
3.60	**0.67**	**0.77**	**0.86**	1.00
7.20	0.81	0.82	0.92	1.00
10.8	0.89	0.91	1.00	**0.98**

Values of greatest combined effect are in bold. Values equal to or less than 0.5 are considered synergistic, from 0.5 to 1.0 are additive, 1.0 to 4.0 are indifferent, and those equal to or greater than 4.0 are considered antagonistic.

FICI values remained within the additive range for all strain–antibiotic–aPDT combinations (Table 1), meaning that the resulting elimination of bacteria consistently yielded greater than baseline effectiveness relative to the sum of fractional MICs. Although no combination reached a truly synergistic qualification, the consistency of improvement displayed with all combinations heralds promise for the future of aPDT applied to an expanded range of ARB and antibiotics. aPDT has been explored but rarely quantified by a fixed metric such as FICI. Similar work has been done before with aPDT and ciprofloxacin (27); blue light therapy (28); and combinations of light therapies, ciprofloxacin, and essential oil extracts (29). Each of these works observes and notes the potential for combined treatment efficacy, although lacks a unified system of synergy assessment.

A short analysis was performed to evaluate the clinical safety of combined aPDT treatment for a localized infection based on necessary photosensitizer concentration and total light exposure. Extrapolation of treatment group MIC enables a judgment check based on expected aPDT dose required to reduce resistance to susceptible levels based on EUCAST breakpoints. This extrapolated exposure value is the minimum dose to

Table 2. Specific *P* values described for each of the statistics presented in Figs. 2 and 4

Figure	Data group	*P* value 1	*P* value 2	*P* value 3
Fig. 2A	Chl: treated	0.1733^{ns}	0.0020**	<0.0001****
Fig. 2A	Tet: treated	0.0531^{ns}	0.0027**	<0.0001****
Fig. 2B	Chl: treated	$>0.9999^{ns}$	0.0428*	<0.0001****
Fig. 2B	Tet: treated	0.4642^{ns}	0.0047**	<0.0001****
Fig. 4A	USA300	0.7898^{ns}	0.0016**	<0.0001****
Fig. 4A	RN4220	0.2097^{ns}	0.0117*	<0.0001****

The left column designates the figure, the second column designates the data within that figure, and the three *P* value columns are represented left to right as seen in Figs. 2 and 4. Data from Fig. 2 were evaluated with a Friedman's test and post hoc Dunn's multiple comparisons test, while Fig. 4 data underwent a Kruskal–Wallis test and post hoc Dunn's multiple comparisons test. For both datasets, ns is not significant; *$P < 0.05$; **$P < 0.01$; ****$P < 0.0001$.

return bacteria to a pseudonatural state of standard antibiotic resistance. For USA300, Chl requires an average exposure of 8.70 J/cm^2, and Tet requires 5.21 J/cm^2. RN4220 treated with Chl requires an average exposure of 10.27 J/cm^2, and Tet requires 3.98 J/cm^2. When applied to localized infections, aPDT is typically employed in much larger doses, both in regard to photosensitizer concentration and total exposure by an order of magnitude (10). Since these minimum combined doses are well below prior clinical applications, combined aPDT and antibiotics poses a feasible method for safely preserving utility of the current antibiotics generation. Additionally, the requirement of many generations to resume resistant state supports the clinical utility of combined aPDT within a realistic time span for antibiotic treatment. A consideration for future utilization is the apparent broadening of MIC distribution as aPDT dose is increased and average MIC decreases in treatment groups (Figs. 1 and 2). MIC distribution may be a topic of interest in larger datasets as complete elimination is important in preventing perpetuation of antibiotic resistance. Still, this distribution broadening positively influences combined aPDT effectiveness due to the increased bacterial population below the susceptible MIC limits in comparison to resistant strains which have a tight distribution that is more difficult to completely eliminate. In this way, even moderate aPDT doses, as presented here, pose a vital opportunity to increase bacterial elimination and aid antibiotic therapies and the immune system in succeeding against dangerous ARB.

Existing literature regarding the combination of aPDT and antibiotic is meager, particularly in evaluation of altered resistances. Even so, it is sufficient for comparison of methods and results to gauge effect consistency and temper mechanism hypotheses. In a study of combined aPDT with methylene blue and antibiotics against *Escherichia coli*, it was observed via electron cryotomography that aPDT produced diffuse microdamage in the envelope as well as promoting membrane vesicle formation (30). Both of these observations directly correlate to increased membrane permeabilization and therefore a reduction in antibiotic resistance. As a demonstration, *Galleria mellonella* larvae inoculated with *E. coli* were found to have improved survival with combined aPDT treatment as compared to individual treatments (30). Another study observed aPDT effects against carbapenem-resistant bacteria, finding a similar reduction in resistance (31). This study also observed an effective impairment of carbapenemase enzyme presence and related genomic toxicity resulting from combined aPDT treatment (31). Overall, these articles support the presented hypothesis that aPDT-induced membrane damage facilitates temporary resistance disruption, as well as the observation that ARB may conduct some form of genomic toxicity, reducing serial recovery of resistance.

Since ARB is a worldwide problem, in which strategies for more effective treatments are sought, our results demonstrate that aPDT, in addition to promoting a reduction in infection, also promotes cellular damage that allows an increase in susceptibility to the antibiotic. The combination of methylene blue as a photosensitizing molecule together with Tet and Chl obtained additive inactivation responses, elucidating that the combination of treatments is the favorable strategy to choose when antibiotic therapy alone is ineffective, as in cases of ARB infection. Methylene blue has shown in vivo activity against various tumors and infections when injected locally and illuminated with red light. However, considering the problem of bacterial resistance to antibiotics, which starts in hospital environments through contact with infected wounds, a possible clinical application could start with the treatment of localized wounds caused by MRSA. Another application would be in the upper airways, in both pharyngotonsillitis and rhinosinusitis, where MRSA can lodge and cause severe respiratory problems; a spray of MB would reach the bacterial cells and thereby be positioned to receive significant photodynamic action (32). Further in-depth study is required to understand the interaction between therapies and mechanisms against the pathogen, in order to obtain effective and optimized protocols. Antibiotics are likely to remain the gold standard of treatment for bacterial infections, but the combination with aPDT may delay the great crisis of antibiotic therapy inefficiency.

Materials and Methods

Bacterial Cultures, Storage, and Preparation.

Sources. All bacteria are strains of *S. aureus*. The strain USA300 was purchased from the American Type Culture Collection, designated TCH1516 (USA300-HOU-MR). The strain RN4220 was obtained through Biodefense and Emerging Infections Research Resources Repository (BEI Resources), National Institute of Allergy and Infectious Diseases (NIAID), National Institutes of Health (NIH): *S. aureus* Fluorescent Reporter Plasmid pSGFPS1, Recombinant in *S. aureus*, NR-51163. The strain ΔSaeR was provided by the Network on Antimicrobial Resistance in *S. aureus* (NARSA) for distribution by BEI Resources, NIAID, NIH: *S. aureus* subsp. aureus, Strain JE2, Transposon Mutant NE1622 (SAUSA300_0691), NR-48164. The strain MW2 in this study is from the National Institute of Standards and Technology (NIST) collection, designated NIST0023. The strain JE2 was provided by NARSA for distribution by BEI Resources, NIAID, NIH: *S. aureus* subsp. aureus, Strain JE2, NR-46543.

Preparation. Glycerol stocks were streaked on Luria-Bertani Agar plates and incubated at 37°C for 16 h, after which an isolated colony is collected with a sterile loop and added to 5 mL cation-adjusted Mueller-Hinton Broth media (MHB). Following overnight incubation of 12 to 16 h at 37°C, concentrated cultures are stored as noted below. Log-phase cultures were prepared by mixing 5 mL of broth medium with 50 μL from overnight cultures and incubating for 5 to 6 h, depending on the strain. These log-phase cultures were used for all experiments unless explicitly noted otherwise. Unless stated otherwise, log-phase cultures were pelleted via centrifuging at 10,000 rpm and 4°C for 2 to 4 min and resuspended in PBS. Optical density measurements at 600 nm (OD_{600}), adjusted for pure medium, were then used for direct dilutions required for experiments.

Storage. Overnight cultures in active use were stored in liquid media at 4°C for a maximum of 4 d in standard culturing tubes. Long-term culture samples were prepared by diluting new overnight liquid culture with glycerol to a concentration of 40% by volume. After gentle mixing, 1 mL of these cultures was distributed into freezer tubes for single-use and stored at −80°C.

Antibiotic MIC Assay.

Antibiotic preparation. Antibiotic stocks stored at 4°C were used in dilution. When used in aPDT treatment, a 4× concentration was created in PBS for

Fig. 6. The (*Left*) plate holder and LED array along with (*Right*) LED driver and power controller.

dilution with the culture and photosensitizer solutions. When applied for culturing, a 2× concentration was created in MHB for dilution with the culture post-aPDT.

MIC protocol. Standard twofold antibiotic serial dilution assays were used as described by Wiegand et al. (33). Briefly, this involves the preparation of antibiotics in MHB, which is diluted across microtiter plate wells containing the same volume of MHB and finished with the addition and gentle aspiration mixing of 2× concentration bacteria with or without methylene blue. Additional samples containing no antibiotic for control and assessment of any significant, unintended aPDT elimination were included. MIC plates were incubated for 16 h at 37°C. MIC plates were visualized with Cytation 5 (BioTek) measurement of OD_{600}. The smallest antibiotic concentrations with no observable growth as compared to pure media were recorded as the MIC value. This was completed in triplicate on three separate occasions for each sample.

Serial MIC passage for resistance recovery. Standard aPDT and MIC procedures are taken for the first round of cultures. Incubation is interrupted every 12 h, at which time the current plate is read and a small sample from the most resistant well in each row is placed in a new MIC plate to continue growth and generation passage. This test is stopped for a strain when all triplicates remain stable for at least two testing periods.

aPDT Protocol.

Photosensitizer. Methylene blue was prepared by thorough dissolution of the dry powder (Sigma-Aldrich, M9140-25G) in pure ethanol. This solution is diluted into PBS to final concentrations of 1 to 4 μM, as required for 2× dilutions with cultures only or 4× dilutions with cultures and antibiotic. In controls, photosensitizer was incubated at large concentrations with strains overnight at 37°C and growth compared to the baseline to evaluate any inherent cytotoxicity or impairing effects not related to either treatment.

Illumination device. Custom equipment was built by Laboratório de Apoio Técnico, Instituto de Física de São Carlos, for uniform and consistent exposure of assay plates (Fig. 6). The plate holder maintains a consistent distance between samples and the underlying light-emitting diode (LED) array. Twenty-four LEDs with reflective cones are arranged in a four-by-six pattern, matching a standard 24-well plate. The LED array is actively cooled by a built-in electric fan and passively by contacting heatsinks. The custom driver and controller board supports current variation to change output intensities to settings of 15, 30, and 45 mW/cm^2. Of these, only 30 mW/cm^2 was used.

aPDT protocol. Log-phase cultures resuspended in PBS were subsequently diluted to $OD_{600} = 0.20$. For each aPDT–antibiotic combination, wells of a 96-well plate were filled with 100 μL of 4× photosensitizer solution. Then, 100 μL of the selected antibiotic in a 4× solution was used for serial dilution across, avoiding the final column for control. Next, 100 μL of 2× culture in PBS, with or without 2× methylene blue included, was then added to all wells and incubated at room temperature in the dark for 1 h. The illuminating device was set up and checked as noted below during incubation. After incubation, samples were gathered prior to exposure and at intervals of 1 or 2 min.

When collecting samples for MIC testing, 10 μL was drawn from each well and placed into wells containing 100 μL MHB volumes with matching antibiotic dilutions at 11/10× concentration to result in exact concentration matches. At this step, samples are split into triplicate for separate antibiotic MIC evaluation in some experiments. This final combination results in an $OD_{600} \approx 0.009$ and an ∼90.9% MHB solution. Plates were incubated for 16 h at 37°C then evaluated as noted in the MIC protocol above.

Bacteria log reduction induced by aPDT was tested following the above protocol through exposure but included samples onto a 10× serial dilution microtiter plate in PBS media. After collection and dilution, these samples were dispensed in 10 μL volumes onto LA plates, incubated for 16 h, digitally imaged, and evaluated for colony forming units per milliliter (CFU/mL) reduction relative to aPDT dosage. This was completed in triplicate on three separate occasions ($n = 9$).

FICI.

FICI calculation. FICI provides a standardized approach in comparing the effects of two treatments that may involve two different MIC assay variable units. The general formula is given as follows (Eq. **1**) (21):

$$FICI_{AB} = FIC_A + FIC_B = \frac{MIC_{AB}}{MIC_A} + \frac{MIC_{AB}}{MIC_B} \quad [1]$$

FIC_x denotes the fractional inhibitory concentration of treatment x in combination divided by that treatment alone. MIC_x denotes the measured inhibitory concentrations of treatment x, with each fraction containing matching units, resulting in a unitless outcome.

$FICI_{AB}$ is the final index value of comparing the two treatments, measured independently by FIC_A and FIC_B. Each individual FIC_n is calculated by the MIC value of n in combination treatment divided by the MIC value of n in individual treatment. In application for comparing antibiotic and aPDT treatments in combination, one fraction is the concentration of antibiotic, and the other is the total delivered energy. The resulting unitless value then determines the utility of combined treatments. Treatments are synergistic if $FICI \leq 0.5$, additive if $0.5 < FICI \leq 1.0$, indifferent if $1.0 < FICI < 4.0$, and antagonistic if $FICI \geq 4.0$ (34, 35).

Data Handling.

Graphing. All graphing and statistics of MIC and CFU data were handled using GraphPad Prism for Windows (36).

MIC and CFU statistical analyses. Analyses of MIC and CFU changes relative to aPDT dose, using the Kruskal–Wallis test and post hoc Dunn's multiple comparisons test, were computed with built-in programs available through GraphPad Prism for Windows (36).

Data, Materials, and Software Availability. All study data are included in the main text.

ACKNOWLEDGMENTS. J.A.W., V.C., and V.V.Y. received partial funding from the NSF (grant CMMI-1826078), the Air Force Office of Scientific Research (grants FA9550-15-1-0517, FA9550-20-1-0366, and FA9550-20-1-0367), Department of Defense (DOD) Army Medical Research (grant W81XWH2010777), NIH (grants 1R01GM127696, 1R21GM142107, and 1R21CA269099), and the Cancer Prevention and Research Institute of Texas (grant RP180588). This work was supported, in part, by the DOD under contract W911NF1920013 to P.d.F. The content of the report does not necessarily reflect the position or the policy of the Government, and no official endorsement should be inferred. V.S.B., K.C.B., and G.K. acknowledge funding from the São Paulo Research Foundation (grants 2013/07276-1, 2018/18188-0, and 2021/09952-0). J.M.S. thanks CAPES finance code 001.

Author affiliations: [a]Biomedical Engineering, Texas A&M University, College Station, TX 77840; [b]Department of Microbial Pathogenesis and Immunology, Texas A&M Health Science Center, Bryan, TX 77807; [c]Institute of Physics of Sao Carlos, University of Sao Paulo, Sao Carlos 13566-590, Brazil; and [d]Department of Veterinary Pathobiology, Texas A&M University, College Station, TX 77843

1. H. Landecker, Antibiotic resistance and the biology of history. *Body Soc.* **22**, 19–52 (2016).
2. X. Zhen, C. S. Lundborg, X. Sun, X. Hu, H. Dong, Economic burden of antibiotic resistance in ESKAPE organisms: A systematic review. *Antimicrob. Resist. Infect. Control* **8**, 137 (2019).
3. Centers for Disease Control and Prevention, *Antibiotic Resistance Threats in the United States 2019* (Centers for Disease Control and Prevention, US Department of Health and Human Services, 2019).
4. A. Chokshi, Z. Sifri, D. Cennimo, H. Horng, Global contributors to antibiotic resistance. *J. Glob. Infect. Dis.* **11**, 36–42 (2019).
5. V. Gupta, P. Datta, Next-generation strategy for treating drug resistant bacteria: Antibiotic hybrids. *J. Dent. Educ.* **76**, 1532–1539 (2012).
6. M. F. Grill, R. K. Maganti, Neurotoxic effects associated with antibiotic use: Management considerations. *Br. J. Clin. Pharmacol.* **72**, 381–393 (2011).

7. V. Fanos, L. Cataldi, Renal transport of antibiotics and nephrotoxicity: A review. *J. Chemother.* **13**, 461–472 (2001).
8. H. Han, H. Yan, K. Y. King, Broad-spectrum antibiotics deplete bone marrow regulatory t cells. *Cells* **10**, 1–9 (2021).
9. S. E. Cosgrove, The relationship between antimicrobial resistance and patient outcomes: Mortality, length of hospital stay, and health care costs. *Clin. Infect. Dis.* **42**(Suppl. 2), 82–89 (2006).
10. J. A. Willis *et al.*, Photodynamic viral inactivation: Recent advances and potential applications. *Appl. Phys. Rev.* **8**, 021315 (2021).
11. N. Ghosh, A. Das, S. Chaffee, S. Roy, C. K. Sen, *Reactive Oxygen Species, Oxidative Damage and Cell Death* (Elsevier Inc., 2017).
12. M. Lan *et al.*, Photosensitizers for photodynamic therapy. *Adv. Healthc. Mater.* **8**, e1900132 (2019).
13. J. P. Tardivo *et al.*, Methylene blue in photodynamic therapy: From basic mechanisms to clinical applications. *Photodiagn. Photodyn. Ther.* **2**, 175–191 (2005).
14. A. F. Dos Santos, D. R. Q. De Almeida, L. F. Terra, M. S. Baptista, L. Labriola, Photodynamic therapy in cancer treatment–An update review. *J. Cancer Metastasis Treat.* **2019**, 10.20517/2394-4722. 2018.83. (2019).
15. J. Clifton II, J. B. Leikin, Methylene blue. *Am. J. Ther.* **10**, 289–291 (2003).
16. P. Dharmaratne *et al.*, Contemporary approaches and future perspectives of antibacterial photodynamic therapy (aPDT) against methicillin-resistant *Staphylococcus aureus* (MRSA): A systematic review. *Eur. J. Med. Chem.* **200**, 112341 (2020).
17. Q. Chen *et al.*, Photodynamic therapy guidelines for the management of oral leucoplakia. *Int. J. Oral Sci.* **11**, 14 (2019).
18. D. J. R. Gusman *et al.*, pH influences the biocompatibility of methylene blue solutions. *Clin. Oral Investig.* **22**, 361–367 (2018).
19. C. Zhang *et al.*, Methylene blue-based near-infrared fluorescence imaging for breast cancer visualization in resected human tissues. *Technol. Cancer Res. Treat.* **18**, 1533033819894331 (2019).
20. The European Committee on Antimicrobial Susceptibility Testing. Breakpoint tables for interpretation of MICs and zone diameters. Version 11.0 (2021). https://www.eucast.org/fileadmin/src/media/PDFs/EUCAST_files/Breakpoint_tables/v_11.0_Breakpoint_Tables.pdf. Accessed 14 March 2022.
21. J. Meletiadis, S. Pournaras, E. Roilides, T. J. Walsh, Defining fractional inhibitory concentration index cutoffs for additive interactions based on self-drug additive combinations, Monte Carlo simulation analysis, and in vitro-in vivo correlation data for antifungal drug combinations against *Aspergillus fumigatus*. *Antimicrob. Agents Chemother.* **54**, 602–609 (2010).
22. A. Wozniak, M. Grinholc, Combined antimicrobial activity of photodynamic inactivation and antimicrobials–State of the art. *Front. Microbiol.* **9**, 930 (2018).
23. M. R. Hamblin, T. Hasan, Photodynamic therapy: A new antimicrobial approach to infectious disease? *Photochem. Photobiol. Sci.* **3**, 436–450 (2004).
24. M. N. Usacheva, M. C. Teichert, M. A. Biel, The role of the methylene blue and toluidine blue monomers and dimers in the photoinactivation of bacteria. *J. Photochem. Photobiol. B* **71**, 87–98 (2003).
25. J. Ghorbani, D. Rahban, S. Aghamiri, A. Teymouri, A. Bahador, Photosensitizers in antibacterial photodynamic therapy: An overview. *Laser Ther.* **27**, 293–302 (2018).
26. I. Chopra, M. Roberts, Tetracycline antibiotics: Mode of action, applications, molecular biology, and epidemiology of bacterial resistance. *Microbiol. Mol. Biol. Rev.* **65**, 232–260 (2001).
27. M. R. Ronqui, T. M. S. F. de Aguiar Coletti, L. M. de Freitas, E. T. Miranda, C. R. Fontana, Synergistic antimicrobial effect of photodynamic therapy and ciprofloxacin. *J. Photochem. Photobiol. B* **158**, 122–129 (2016).
28. G. Fila, A. Kawiak, M. S. Grinholc, Blue light treatment of *Pseudomonas aeruginosa*: Strong bactericidal activity, synergism with antibiotics and inactivation of virulence factors. *Virulence* **8**, 938–958 (2017).
29. N. L. F. Pereira *et al.*, Antibacterial activity and antibiotic modulating potential of the essential oil obtained from *Eugenia jambolana* in association with led lights. *J. Photochem. Photobiol. B* **174**, 144–149 (2017).
30. A. S. Garcez *et al.*, Effects of antimicrobial photodynamic therapy on antibiotic-resistant *Escherichia coli*. *Photodiagn. Photodyn. Ther.* **32**, 102029 (2020).
31. Y. Feng, A. Palanisami, S. Ashraf, B. Bhayana, T. Hasan, Photodynamic inactivation of bacterial carbapenemases restores bacterial carbapenem susceptibility and enhances carbapenem antibiotic effectiveness. *Photodiagn. Photodyn. Ther.* **30**, 101693 (2020).
32. K. C. Blanco, A. P. da Silva, V. H. Panhoca, L. T. Moriyama, V. S. Bagnato, Photodynamic therapy of adenoid hypertrophy in acute rhinosinusitis. *Photodiagn. Photodyn. Ther.* **39**, 102892 (2022).
33. I. Wiegand, K. Hilpert, R. E. W. Hancock, Agar and broth dilution methods to determine the minimal inhibitory concentration (MIC) of antimicrobial substances. *Nat. Protoc.* **3**, 163–175 (2008).
34. F. C. Odds, Synergy, antagonism, and what the chequerboard puts between them. *J. Antimicrob. Chemother.* **52**, 1 (2003).
35. X. Xu *et al.*, Synergistic combination of two antimicrobial agents closing each other's mutant selection windows to prevent antimicrobial resistance. *Sci. Rep.* **8**, 7237 (2018).
36. GraphPad Software (GraphPad Software, Inc., San Diego, CA). https://www.graphpad.com. Accessed 2 November 2021.